Macromolecules

Article

pubs.acs.org/Macromolecules

Strong Ligand–Block Copolymer Interactions for Incorporation of Relatively Large Nanoparticles in Ordered Composites

Yue Gai, Ying Lin, Dong-Po Song, Benjamin M. Yavitt, and James J. Watkins*

Department of Polymer Science and Engineering, University of Massachusetts Amherst, 120 Governors Drive, Amherst, Massachusetts 01003, United States

Supporting Information

ABSTRACT: For well-ordered block copolymer (BCP) nanocomposites containing nanoparticles (NPs), the ratio of NP core diameter (d_{core}) and BCP domain width (L) has been generally limited with $d_{core}/L < 0.3$ when NP/BCP interactions are relatively neutral or weak. Here, we systematically investigate the spatial distribution of gold nanoparticles (NP) ranging in size up to 0.8 times that of the target domain width in symmetric polystyrene-*b*-poly(2-vinylpyridine) (PS-*b*-P2VP) using a hydrogen-bonding-mediated (H-bonding) assembly. NPs with core diameters (d_{core}) 2, 5, 9, and 15 nm are coated with ligands bearing phenol groups as the hydrogen-donating sites for H-bonding including 2-(11-mercaptoundecyl)hydroquinone and thiol-terminated poly(4-hydroxystyrene). These hydroxylated NPs are selectively incorporated into the P2VP block (domain width L = 7−37 nm) over a wide range of volume fractions (ϕ = 3−26 vol %). Particle distributions are biased toward the center of in the P2VP domains when d_{core}/L is greater than 0.3 and are otherwise uniformly distributed within the target domain. The H-bonding interactions between NP and BCP provide favorable enthalpic interaction to overcome the inherent entropy penalties mainly arising from polymer chain stretching upon the sequestration of large particles. This strong thermodynamic driving force provides a means of incorporating relatively large NPs within BCP templates to further enable the preparation of well-ordered composites that can take advantage of the attractive size-dependent properties of NPs.

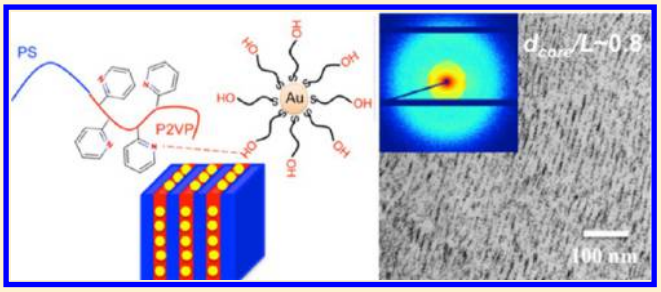

INTRODUCTION

Well-ordered block copolymer (BCP) nanocomposite containing inorganic nanoparticles (NP) are of great interest as next-generation functional materials with enhanced electronic, optical, and magnetic properties.[1−8] The performance of such hybrid materials fundamentally depends on precise control of the spatial organization of the NPs that offer attractive physical properties as determined by particle size, shape, and filling fraction.[1,3] For example, localized surface plasmon resonance (LSPR) and quantum emission of semiconductor NPs displaying size-dependent properties have been applied in biosensing and solar energy harvesting.[9−14] Recent development of fine control over NP sizes from a few to tens of nanometers provides new opportunities for fabricating novel functional block polymer-based composite.[15−22]

The spatial distribution of particles in a linear BCP is determined by a delicate thermodynamic balance between enthalpy and entropy.[1,2,23,24] The enthalpic contribution arises from the interaction of NP with specific block. Particularly for large NPs, the entropic contributions are often dominated by polymer chain stretching penalties while particles translation entropy is more dominant for smaller NPs.[24−28] Recent work has shown that surface modification of small NPs with d_{core} from 2 to 3 nm is a facile strategy to localize the NPs selectively within a BCP target domain (domain width L) at d_{core}/L less than 0.2.[29−33] However, by either increasing the loading of such small enthalpically neutral particles or by incorporating large particles with d_{core} over 10 nm, the entropic penalties push the system toward a disorder state. In contrast, by introducing functional groups on the NP surfaces that exhibit strong interactions with one block of the BCP,[34−39] the favorable enthalpic interactions between NPs and corresponding block enable the very high loading more than 40 wt % of NPs to alleviate the BCP chain stretching penalty while maintaining the strong phase segregation in the composite.[36]

In spite of successful selective loading small NPs within linear BCPs, it remains challenging to integrate large NPs with core diameter greater than 10 nm into BCP or maintain well-ordered composites structures with d_{core}/L greater than 0.3. Recently, our group has demonstrated the directed assembly of large NPs over 15 nm using an amphiphilic brush BCP with a large domain widths up to 150 nm as the template.[40] Surprisingly, very little work has been directed to incorporating relative large NP into smaller linear BCP domain by employing favorable interaction between NP and BCP.

Received: December 1, 2015
Revised: April 7, 2016
Published: April 27, 2016

DOI: 10.1021/acs.macromol.5b02609
Macromolecules 2016, 49, 3352−3360

Scheme 1. Illustration of Coassembly of Hydroxylated Au NPs with PS-*b*-P2VP through H-Bonding between Ligands on Gold and P2VP Block of the BCP

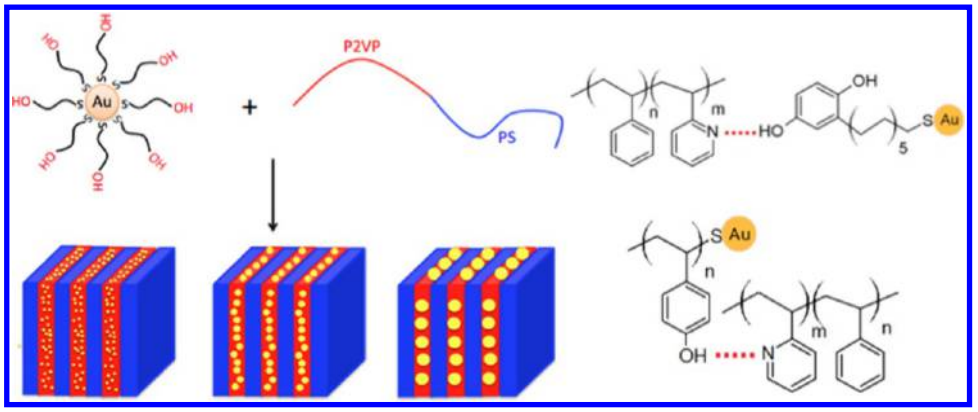

NP organization with weak or neutral interaction has been studied both theoretically and experimentally. Thompson et al.[25] predicted that for NPs chemically compatible with the A block of an A−B BCP system larger NPs ($d_{core}/L \sim 0.3$) prefer to localize at the center of A domain, while smaller NPs ($d_{core}/L \sim 0.2$) were preferentially distributed at the interface of the two domains. Bockstaller et al.[26] experimentally observed trends consistent with these simulations by introducing particles modified with aliphatic ligands into poly(styrene-*b*-ethylene-propylene) (PS-*b*-PEP). Gold NPs with $d_{core}/L \sim 0.06$ segregated to the intermaterial dividing surface and silica NPs with $d_{core}/L = 0.26$ mostly localized in the center of the PEP domain. Chiu et al.[30] reported a more systematic study in which PS-capped gold NPs were incorporated into symmetric PS-*b*-P2VP BCP with d_{core}/L ranging from 0.035 to 0.12. Particles were localized in the center of the PS domain, and their Gaussian distribution width became more narrow with increasing loading of NPs or with decreasing domain width. Although the distribution of the enthalpically neutral modified NPs within the BCP was studied in detail, the weak interaction between NPs and BCP ultimately limited d_{core}/L less than 0.3. It is of great interest both from fundamental and application viewpoints to investigate systematically the potential for achieving well-ordered composites with substantially higher d_{core}/L in linear BCP using hydrogen-bonding-mediated assembly.

We report the assembly of hydroxylated gold NPs within linear PS-*b*-P2VP and quantify preferential NP segregation in terms of particle core size versus domain width (d_{core}/L). We synthesize Au NPs with diameters of 2, 5, 9, and 15 nm, and either 2-(11-mercaptoundecyl)hydroquinone or thiol-terminated poly(4-hydroxystyrene) (PHOST) serves as hydrogen-bonding donor ligand. Pyridine units of the P2VP in symmetric PS-*b*-P2VP function as a hydrogen-bonding acceptor as illustrated in Scheme 1. We also integrate large NPs ($d_{core} \sim 15$ nm) into linear BCPs, which have been rarely reported.

EXPERIMENTAL SECTION

Materials. Sodium borohydride, dodecanethiol (>98%), 2-(11-mercaptoundecyl)hydroquinone (short for hydroquinone) (95%), acetoxystyrene (96%, inhibitor removed by base aluminum oxides before usage), azobis(isobutyronitrile) (98%, recrystallized before use), and hexylamine (99%) were purchased from Sigma-Aldrich; tetra-*n*-octylammonium bromide (98%), hydrogen tetrachloroaurate (100%, for traces of metal analysis), octadecanethiol (96%), 2-cyano-2-propyl benzodithioate (97%), and aluminum oxide basic Brockmann I for chromatography 50−200 μm, 60A, were bought from Acros Organics; sodium citrate (99%−101%) was from Fisher Bioreagents. Hydrochloric acid, ammonium hydroxide, acetic acid, toluene, methanol, ethanol, ethyl ether, hexane, tetrahydrofuran (THF), and *N*,*N*-dimethylformamide (DMF) (99.8%) were purchased with guaranteed grade. Symmetric PS-*b*-P2VP block copolymers were obtained from Polymer Source, Inc. (Montreal, Canada). The properties of each block copolymer are listed in Table 1.

Table 1. Molecular Information for Block Copolymers Used for Assemblies

PS-*b*-P2VP	M_n (kg/mol)	P2VP (vol %)	M_w/M_n	L_{P2VP} (nm)
8.2K-*b*-8.3K	16.5	50.3	1.09	7.1
25K-*b*-25K	50	50.0	1.06	15.1
40K-*b*-44K	84	52.4	1.10	25.1
102K-*b*-97K	199	48.7	1.12	36.9

Controlled Synthesis of Size-Tunable Au NPs. Core diameter 2 nm Au NPs modified with hydroquinone were synthesized following established Brust[15] one-phase procedures by replacing methanol with THF. Hydroquinone-capped Au NPs with $d \sim 5-9$ nm were produced by Miyake et al.[16,22] heat treatment, followed by ligand exchange. Au NPs with core diameter ~15 nm were prepared based on the one-step water phase Turkevich[41] synthesis procedure. The capping agent sodium citrate was then replaced by PHOST and hydroquinone to disperse Au NPs in DMF. PHOST synthesis followed the routine used in previous work.[40] All Au NPs were filtered through 0.2 μm PTFE filter (bought from VWR) before further usage. More experimental details including particles synthesis and ligand exchange are stated in the Supporting Information.

PS-*b*-P2VP/Au Composite Fabrication. Au NPs of core diameter from 2 to 15 nm with weight fractions from 0.1 to 0.5 were dissolved in freshly prepared PS-*b*-P2VP (2 wt %) solution in selective solvent as stated in the Supporting Information. Bulk films of NP/BCP composites were prepared by drop-casting the solution of NP/BCP blends onto glass slides and then drying at room temperature. The composites were then annealed in saturated chloroform solvent vapor at room temperature for at least 2 days and slowly dried in air for 1 day.

Au NP Characterization. The core diameters of Au NPs were characterized by transmission electron microscopy (TEM, JEOL 2000FX, 200 kV) by dropping a dilute nanoparticle solution onto a thin carbon film supported by a cooper grid. Au NP size distributions, and corresponding histograms were analyzed for a sample size of 300−400 particles with standard image analysis software (ImageJ). Fourier transform infrared (FT-IR) (PerkinElmer 2000) spectra of ligands and nanoparticles were taken in the range from 4000 to 650 cm^{-1} in ATR mode. The weight fraction of the gold core was measured by thermogravemetric analysis (TGA, TA Instruments Q500) from 20 to

DOI: 10.1021/acs.macromol.5b02609
Macromolecules 2016, 49, 3352−3360

800 °C at 10 °C/min under air purge flow. The mean areal hydroxyl group densities of Au NPs were calculated from the particle surface area and Au core weight fraction (Table 2).

Table 2. Properties of Au NPs (a–d) Capped with Hydroquinone and (e) Coated with PHOST in Figure 1.

NP	aver d_{core} (nm)	core weight (%)	ligand density (per nm^2)	hydroxyl group density (per nm^2)
NP-1.81	1.80	19.5	48.8	97.6
NP-5.70	5.70	29.2	90.3	181
NP-8.87	8.87	40.8	83.5	167
NP-15.3	15.3	10.6	843	1690
NP-16.0	16.0	67.2	4.70	118

PS-*b*-P2VP/Au NP Composite Characterization. Morphology and domain spacing of neat block copolymer and NP/BCP blends were characterized using small-angle X-ray scattering (SAXS). Bulk films of PS-*b*-P2VP/Au NPs were scraped from glass slides and placed evenly in the center of a metal washer sandwiched by Kapton tape. These samples were measured on Ganesha SAXS-LAB (UMass Amherst) with Cu Kα 0.154 nm line on SAXS or ESAXS mode. Room-temperature microtoming (Leica Ultracut microtome) was used to cut the nanocompsite bulk film into 50 nm thin films and sections collected using a carbon film supported by copper grids. For the samples containing d_{core} ~ 9–15 nm Au NPs, subsequent iodine selective staining was applied to P2VP domains to improve PS/P2VP domain contrast. The prepared thin films of NP/BCP composites were then characterized by TEM (JEOL 2000FX, 200 kV).

RESULTS

Size Distribution of Au NPs and Ligand Density. Au NPs mean core diameters (d_{core}) and standard deviations are presented in Figure 1. FT-IR spectra (Figure 2) of nanoparticles resemble that hydroquinone or PHOST ligands bound to the particles' surfaces. A less intense S–H band at 2550 cm^{-1} is present in the spectrum of the hydroquinone ligand and is not evident in hydroquinone-capped Au NPs spectra, indicating that the thiol bond has dissociated while the Au–S bond formed. The broad peak at 3300–3400 cm^{-1} suggests the existence of hydroxyl groups on the NPs surface (Figure 2A). Complete de-esterification of poly(4-acetoxystyrene) is indicated by the disappearance of C=O characteristic band at 1755 cm^{-1} as well as the presence of a broad O–H peak at 3300 cm^{-1} in the spectrum of PHOST (Figure 2B).[40] The appearance of the characteristic band of PHOST in the NP spectrum indicates the successful attachment of PHOST onto the NPs surfaces.

Au NPs ligand densities are listed in Table 2. The calculations are based on core weight fraction measured by TGA, the number of hydroxyl groups per unit of PHOST (~25, PHOST M_n ~ 3.2 kg/mol, PDI ~ 1.09) and hydroquinone (~2), and the densities of the components[36,40] (PS-*b*-P2VP ~1.05 g/cm^3, gold ~19.3 g/cm^3, PHOST ~1.16 g/cm^3, and hydroquinone ~1.052 g/cm^3; calculations are stated in the Supporting Information). To estimate and compare the effective enthapic contributions to the system, the number of hydrogen-bonding groups per volume for each type of NP was normalized (Figure 2D). Hydroxyl group density is particularly higher for NP-15.3 due to the ineffective stabilization of large NPs with a small molecule thiol. To avoid NPs aggregation, the addition of excess hydroquinone inevitably leads to the presence of free ligands and thus an increase in the number of H-bonding donor groups (both free and bound). We also noticed that using the number of hydroxyl group to estimate

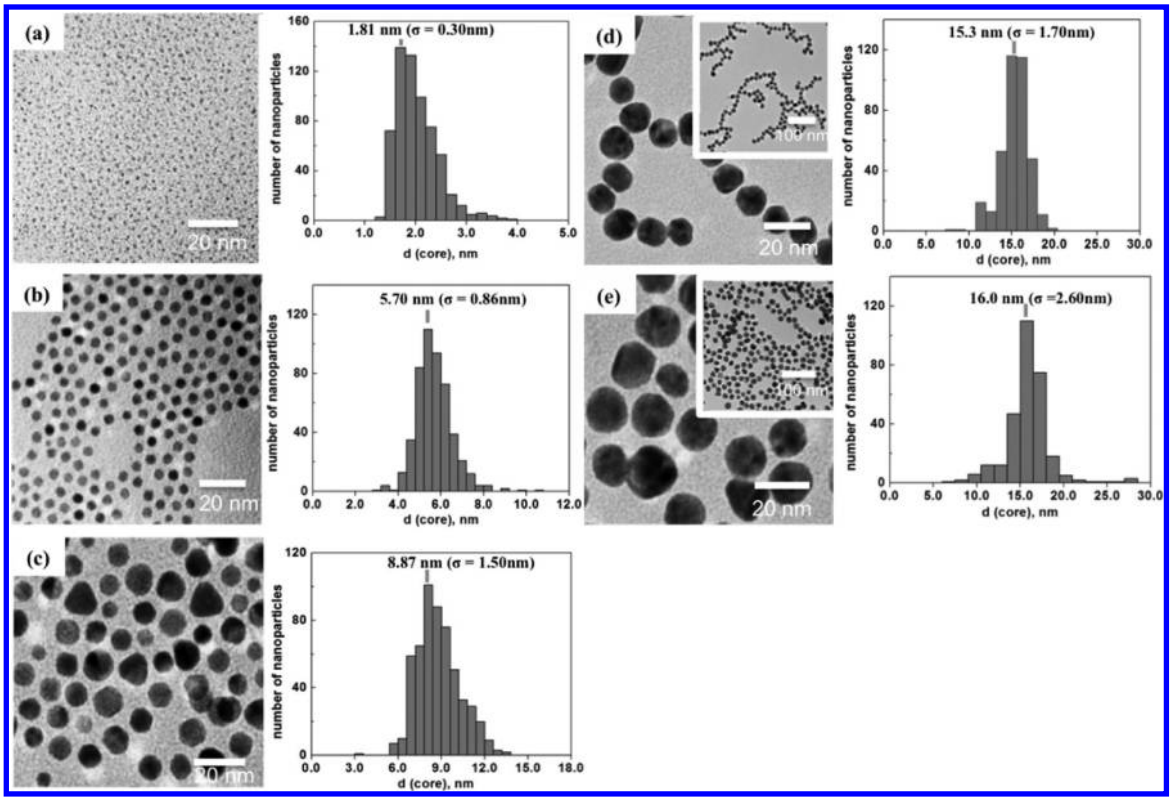

Figure 1. TEM images and core diameter histograms of synthesized hydroxylated gold NPs; hydroquinone stabilized Au NPs (a) 1.81 ± 0.30, (b) 5.70 ± 0.86, (c) 8.87 ± 1.50, and (d) 15.3 ± 1.70 nm. (e) PHOST-capped Au NPs 16.0 ± 2.60 nm accordingly.

DOI: 10.1021/acs.macromol.5b02609
Macromolecules 2016, 49, 3352–3360

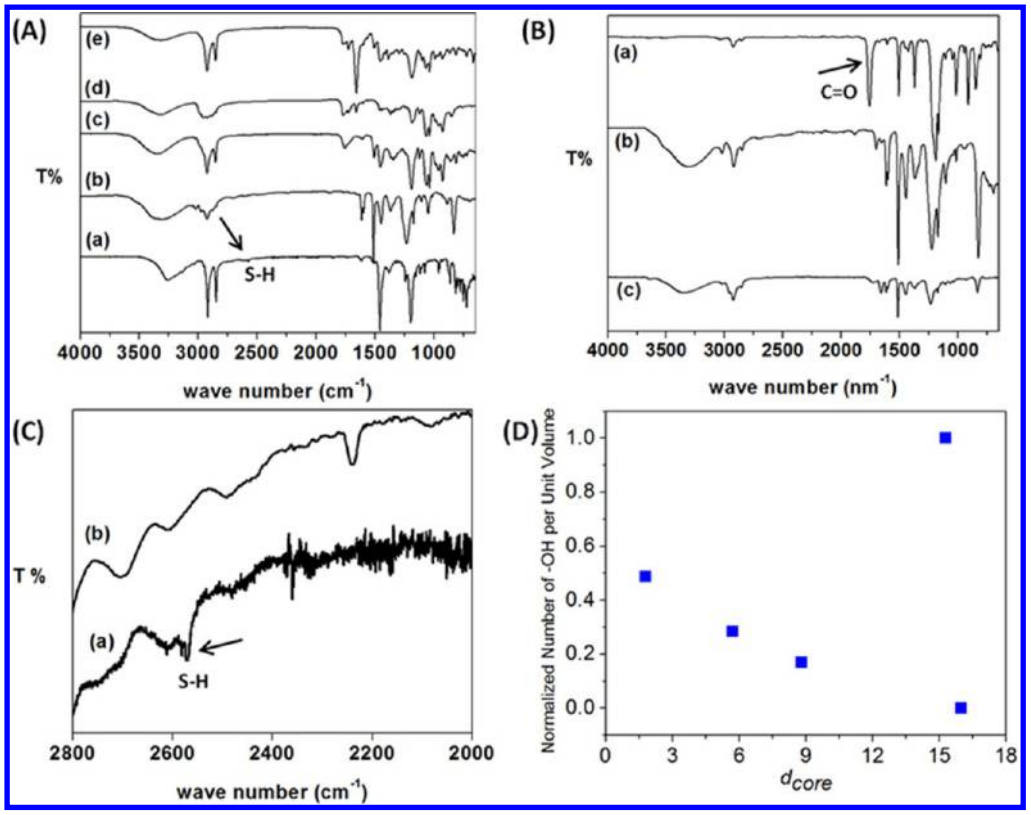

Figure 2. FT-IR spectra of sets (A): (a) Hydroquinone, hydroquinone-coated Au NPs with average size (b) 1.81, (c) 5.70, (d) 8.87, and (e) 15.3 nm. FT-IR spectra of sets (B): (a) poly (4-acetoxystyrene), (b) poly (4-vinylphenol) (PHOST) and (c) PHOST-coated Au NPs with d_{core} = 16.0 nm. (C) Magnified area of S−H peak as shown in (A). (D) Plot of normalized number of hydrogen bonding group per unit volume vs Au NPs core diameter; for calculation see the Supporting Information.

the enthapic contribution has several issues. For example, the H-bonding has direction and saturation; the number of hydroxyl groups is more than the number of hydrogen bonding between particles and block copolymer due to particles self-interaction and existence of free ligand. In spite of these issues, earlier work[34−36,40] reported that the favorable H-bonding interactions between NPs and corresponding block enhanced the microphase segregation to alleviate the BCP chain-stretching penalty in different systems. The hydroxyl group density of ligand-stabilized Au NPs in this system is high enough to yield adequate interaction with the P2VP domain.

Au NP Spatial Organization in BCP in Terms of d_{core}/L. To demonstrate NPs distributions, TEM images of composite samples prepared by microtoming are presented for a range of particle core diameters (d_{core}) and P2VP domain widths L (Figure 3). Consider the assembly of $d_{core} \sim 1.81$ nm Au NP/BCP as one example (Figure 3a−d); the d_{core}/L ratios for these samples are less than 0.3 (from 0.049 to 0.25). The samples containing the 1.8 and 5.7 nm NPs are unstained, and contrast in the images only comes from the electron density difference between metal core and polymer matrix. With core diameter increasing to 5.70 nm, NPs become centralized in the domain with d_{core}/L greater than 0.3 but remain uniformly distributed in larger domains at which d_{core}/L is 0.23 and 0.15 (Figure 3e−h). The incorporation of 5.70 nm NPs into 7.1 nm domains resulting in a significantly increasing d_{core}/L to 0.8 in NP/BCP assembly with an interparticle distance less than 10 nm is noteworthy. Larger NPs (samples are then stained with iodine to increase domain contrast) are more apparently pushed toward the center of the P2VP domains for most d_{core}/L ratios greater than 0.3 (Figure 3i−p).

Figures 3a,e,i,m confirm the particles distribution transition, in which the particles are pushed toward to center of domain with increasing d_{core}/L. For NP-8.87, which has a core diameter slightly larger than the P2VP domain size (7.1 nm), Y-shape defects occur in the nanocompostie (Figure 3i). In Figure 3m, NPs are expelled out of the polymer domain with d_{core}/L over than 2, while the BCP maintains its lamellar structure.

Figure 4 show that linear block copolymer templates direct the distribution of $d_{core} \sim 16.0$ nm PHOST-coated Au NPs. The NPs are by definition larger than the block domain at $d_{core}/L \sim 2$ but clearly reside at the center of the domain with $d_{core}/L \sim 0.64$. A lamellar morphology is observed with a d_{core}/L of 0.4, and particles are not restricted to center of the P2VP domain. Figures 3 and 4 suggest that large NPs ($d_{core} \sim 15$ nm) distributions in linear BCP are mainly dependent on relative size between NPs and block domain rather than their surface stabilizer.

The corresponding SAXS spectra are shown in Figure 5, and domain spacing is calculated from the primary order peak. Unfortunately, SAXS (Figure 5D) does not provide structure information for NP-15.3 and BCP composite. The high scattering cross section of the 15 nm Au NPs produces strong background scattering and makes resolution of signal generated from the NP/BCP blends quite difficult.

Au NP Distribution in BCP in Terms of NP Loading. Figure 6 shows NP distribution with increasing loading of Au NPs. PS(25K)-*b*-P2VP(25K) BCP forms an ordered lamella structure with up to 26 vol % (30 wt %) $d_{core} \sim 1.81$ nm Au

DOI: 10.1021/acs.macromol.5b02609
Macromolecules 2016, 49, 3352−3360

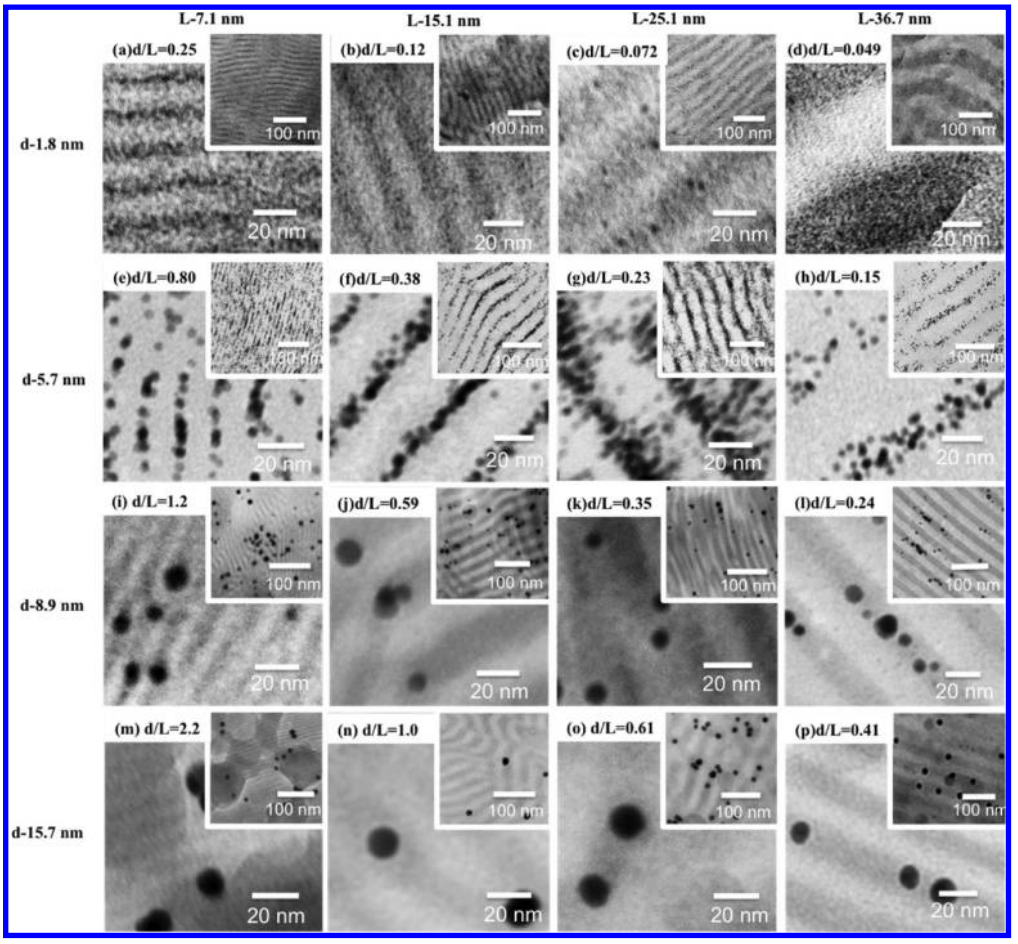

Figure 3. TEM images of NP-1.81 blends with linear symmetric PS-*b*-P2VP of M_n (total) (a) 16.5, (b) 50, (c) 84, and (d) 199 kg/mol. NP-5.70 blends with linear symmetric PS-*b*-P2VP of M_n (total) (e) 16.5, (f) 50, (g) 84, and (h) 199 kg/mol. NP-8.87 blends with linear symmetric PS-*b*-P2VP of M_n (total) (i) 16.5, (j) 50, (k) 84, and (l) 199 kg/mol. NP-15.3 blends with linear symmetric PS-*b*-P2VP of M_n (total) (m) 16.5, (n) 50, (o) 84, and (p) 199 kg/mol. NPs volume fraction (including organic component) ∼9−17 vol % (20 wt % from (a) to (l), 10 wt % from (m) to (p)); see Supporting Information for details. In images (i)−(p) the P2VP domains, which appear gray, are lightly stained with iodine.

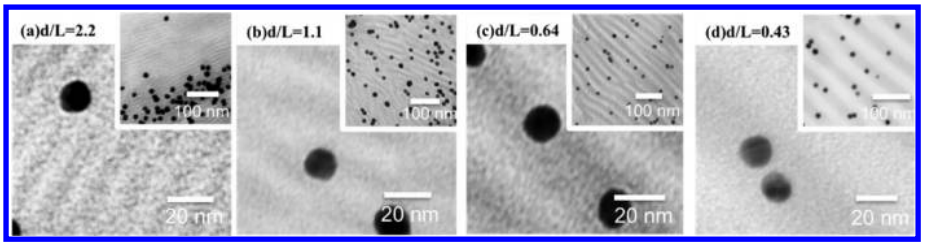

Figure 4. TEM images of NP-16.0 blends with linear symmetric PS-*b*-P2VP of M_n (total) (a) 16.5, (b) 50, (c) 84, and (d) 199 kg/mol. NPs volume fraction ∼4 vol % (10 wt %). The P2VP domains are lightly stained with iodine to increase domain contrast.

NPs but undergoes a morphology transition at a NP loading concentration of 35 vol % (40 wt %). The system is disordered upon incorporation of 45 vol % (50 wt %) Au NPs. As no staining is used in these samples, the high contrast from gold core indicates that the NPs are uniformly distributed in block domain in regardless of loading.

Figures 6f−j show the structure of NP-5.70 within PS(25K)-*b*-P2VP(25K) BCP composite. Well-ordered lamellar structures are observed again by incorporating up to 24 vol % (30 wt %). Au NPs and the Au NPs self-aggregate at NPs loadings over 28 vol % (40 wt %). We also note that the NPs are centralized within the target domain at low loading and gradually spread to the domain edges as more particles are loaded in the BCP. The structure of NP-16.0 and PS(40K)-*b*-P2VP(44K) nanocomposites are shown in Figures 6k−n. It is noteworthy to point out the lamellae structure at NPs loading less than 8 vol % (20 wt %), confirming that the linear block copolymer is useful as a template to guide large NPs assemblies.

Figure 7 shows a shift of the primary peaks to lower q values with the increasing loading of NPs, indicating a swelling of the target domains due to a selective incorporation of NPs within P2VP domains. As shown in Figure 7A, the domain spacing was increased from 30 to 40 nm as calculated according to the q values for the primary peak ($d = 2\pi/q^*$). A symmetric lamellar morphology formed in the neat BCP sample as indicated by the higher order reflections at $3q$. In contrast, an asymmetric lamellar morphology was observed in the composite samples containing NPs 8−26 vol % (10−30 wt %). Moreover, a

DOI: 10.1021/acs.macromol.5b02609
Macromolecules 2016, 49, 3352−3360

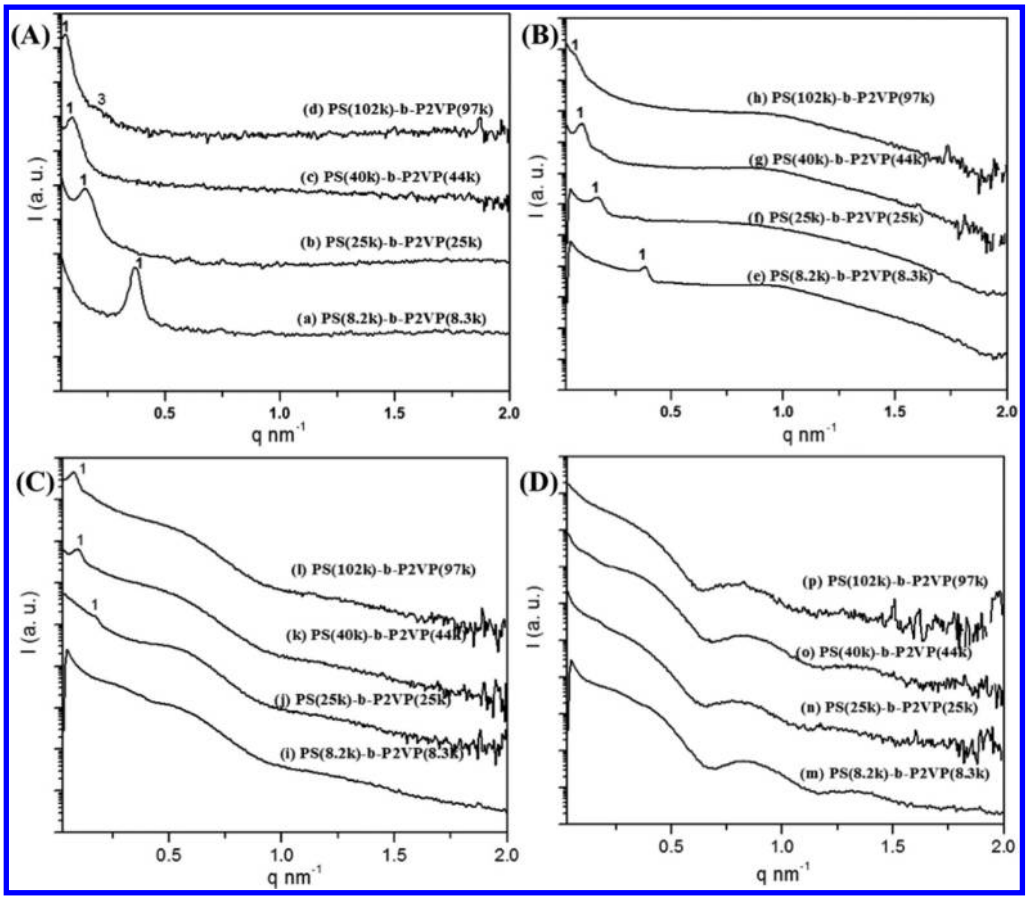

Figure 5. SAXS spectra of: (A) NP-1.81 blends with linear symmetric PS-*b*-P2VP of M_n (total) (a) 16.5, (b) 50, (c) 84, and (d) 199 kg/mol. (B) NP-5.70 blends with linear symmetric PS-*b*-P2VP of M_n (total) (e) 16.5, (f) 50, (g) 84, and (h) 199 kg/mol. (C) NP-8.87 blends with linear symmetric PS-*b*-P2VP of M_n (total) (i) 16.5, (j) 50, (k) 84, and (l) 199 kg/mol. (D) NP-15.3 blends with linear symmetric PS-*b*-P2VP of M_n (total) (m) 16.5, (n) 50, (o) 84, and (p) 199 kg/mol. NPs volume fraction (including organic component) 9−17 vol % (20 wt % from (a) to (l), 10 wt % from (m) to (p)); see Supporting Information for details.

morphology transition from lamellae to cylinder was achieved at a high NP loading of up to 35 vol % (40 wt %) (Figure 7A). A further increasing of NP loading to 45 vol % (50 wt %) resulted in a disordered state. Upon addition of larger NPs (Figure 7B), self-aggregation occurs, and phase segregation and order within the composites are compromised, as verified by more intense NPs scattering intensity and a less intense first-order peak at 42 vol % (50 wt %) loading of NPs.

DISCUSSION

A number of studies have explored the thermodynamic balance of NP/BCP assemblies.[1−3,23,25,42] Generally, the enthapic contribution is governed by the interactions between the NPs and BCPs, while the entropic contribution is influenced by polymer chain stretching as well as NP translation upon mixing. H-bonding meditated assembly provides favorable enthalpic interactions that can promote strong phase segregation in the NP and BCP composite. Figure 8 summarizes the nature and distribution of NPs in the composites at specific d_{core}/L values based on TEM image analysis.

The behavior can be summarized as follows:

- For $0 < d_{core}/L < 0.3$, the favorable enthalpic interactions effectively offset the entropy penalty, and the relatively small NPs are easily accommodated up to relatively high NP loadings. The NPs are uniformly distributed in the target domain. And the uniform distribution in selective domain differs from systems with relatively weak interactions in which NPs distribution is biased toward the center of the target (d_{core}/L up to 0.12).[29,30] The surface modification of neutral or mixture ligand may also introduce particles located at the interface of two domains at low d_{core}/L (less than 0.2), also significantly different from a H-bonding interaction system with selective incorporation of nanoparticles.[26,33]
- At $0.3 < d_{core}/L < 0.5$, as the relative NP size increases; entropy begins to play a prominent role in the spatial organization of the NPs. Initially, with low loading of NPs, the NPs distribute toward the center of the target domain in order to reduce entropic penalty by minimizing chain stretching through localization near chain ends.[23,23,25] The favorable enthalpic contributions of the strong interactions enable the incorporation of additional NPs into the domain, but the NPs have to increasingly be accommodated in less preferred regions near the domain edges. Once NPs saturate the domain further addition of NPs results in aggregation and macrophase separation.
- At $0.5 < d_{core}/L < 1$, entropic penalties become significant and begin to dominate as the NPs size becomes comparable to the domain width. While the favorable interactions enable the accommodation of NPs within the target domains, the loadings concentrations are not as high as those of composite containing smaller NPs. Our experimental results indicate that well-ordered lamellar morphologies can be observed in NP/BCP

DOI: 10.1021/acs.macromol.5b02609
Macromolecules 2016, 49, 3352−3360

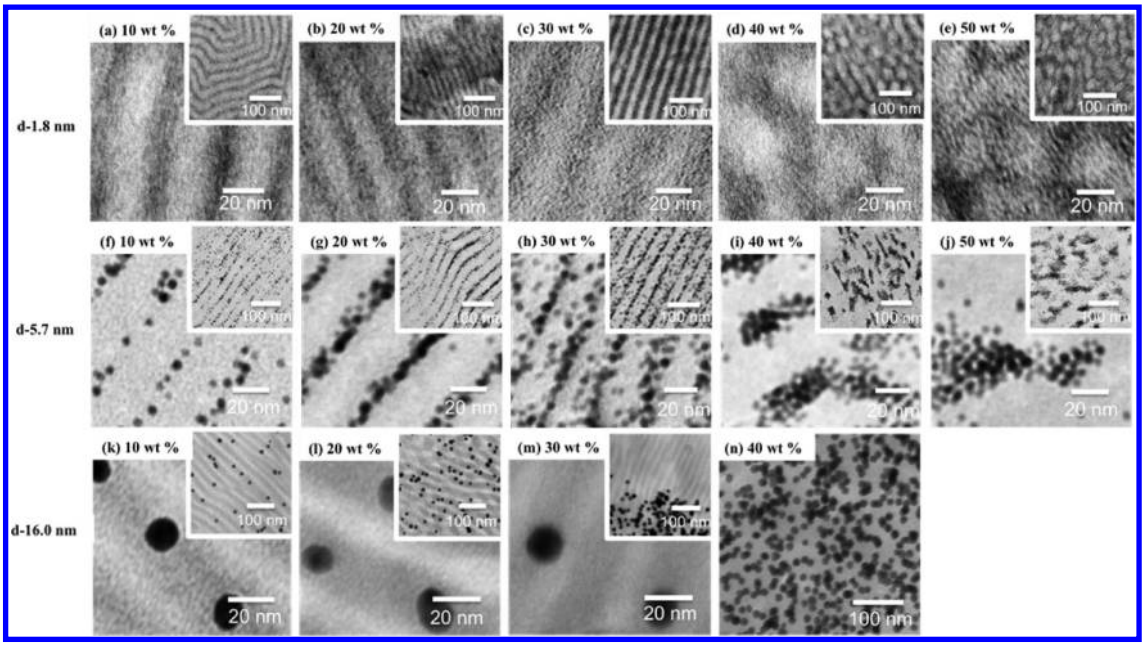

Figure 6. TEM images of NP-1.81 blends with PS(25K)-*b*-P2VP(25K) ($d_{core}/L \sim 0.12$) with NPs volume fraction (including organic component) from 8 to 45 vol %: (a) 10, (b) 20, (c) 30, (d) 40, and (e) 50 wt %. TEM images of NP-5.70 blends with PS(25K)-*b*-P2VP(25K) ($d_{core}/L \sim 0.38$) with volume fraction (including organic component) from 7 to 42 vol %: (f) 10, (g) 20, (h) 30, (i) 40, and (j) 50 wt %. TEM images of NP-16.0 blends with PS(40K)-*b*-P2VP(44K) ($d_{core}/L \sim 0.61$) with NPs volume fraction (including organic component) from 4 to 18 vol %: (k) 10, (l) 20, (m) 30, and (n) 40 wt %; samples from (k) to (n) are stained with iodine to increase domain contrast. Ordered structured remained with NPs volume fraction up to ~25 vol % (with organic ligands), and details are stated in the Supporting Information.

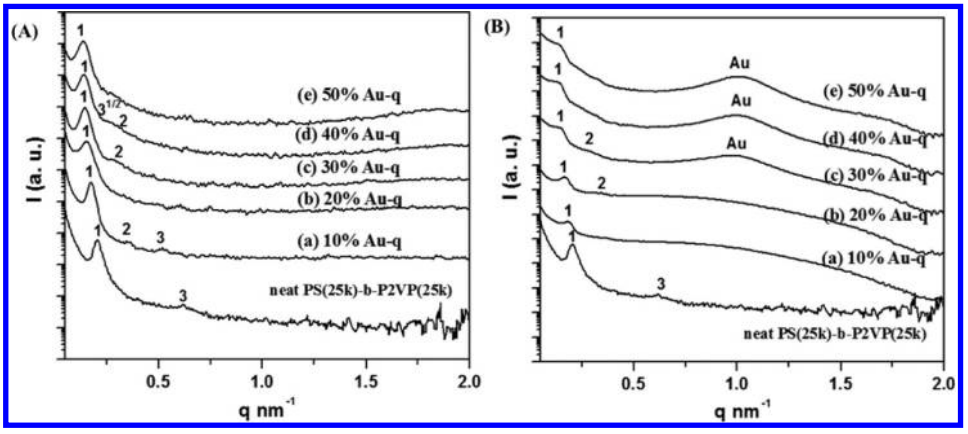

Figure 7. (A) SAXS spectra of blends of PS(25K)-*b*-P2VP(25K) with NP-1.81 at different volume fractions (including organic component) from 8 to 45 vol %: (a) 10, (b) 20, (c) 30, (d) 40, and (e) 50 wt % with $d_{core}/L \sim 0.12$. (B) SAXS profiles of blends based on the same BCP containing NP-5.70 ($d_{core}/L \sim 0.38$) with NPs volume fraction (including organic component) from 7 to 42 vol %: (a) 10, (b) 20, (c) 30, (d) 40, and (e) 50 wt %.

blends at $d_{core}/L \sim 0.8$ with less than 15 vol % (20 wt %) NP loadings (Figure 3e).

- At $1 < d_{core}/L$, NPs with core diameter size similar or larger than domain width increase the NP/BCP mixture entropy significantly. Under these conditions, the distortion of domain and chain stretching required to incorporate the NPs causes X, Y, or T shape defects, consistent with simulation results.[43] In many cases, NPs are expelled out of the domain as free energy does not favor the assembly and NPs only attach interface of the two blocks by hydrogen-bonding interaction.

■ CONCLUSIONS

Hydroxylated Au nanoparticles with narrow size distributions have been synthesized over a wide range of particle diameters and selectively incorporated within the target domains of linear block copolymers to reveal NP spatial distribution in composites with hydrogen-bonding interactions between the NPs and BCP chain segments. At small values of $d_{core}/L \sim 0.1$, the particles are nearly homogeneously distributed within the target domains. As particle size increases relative to the target domain width (d_{core}/L over 0.3), the NP locations are initially biased toward he domain center at low concentrations and then are accommodated in less energetically preferred locations nearer the domain boundaries as NP loading increases. Favorable enthalpy introduced by H-bonding interaction offset entropy penalty mainly from chain stretching upon incorporation of large NPs. We successfully employ symmetric linear block copolymer as template to incorporate 15 nm Au NPs and increase d_{core}/L to 0.8 while maintaining well-ordered lamellar structure in NP/BCP composites. This systematic study provides a guide for a precise control on NP-size-tunable

DOI: 10.1021/acs.macromol.5b02609
Macromolecules 2016, 49, 3352−3360

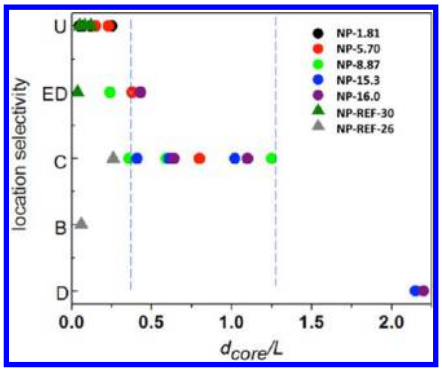

Figure 8. (a) Relationship between d_{core}/L and NPs location as indicated by labels: U = uniform distribution, ED = edge diffused, C = centered distribution, B = interface/boundary of domain, D = disorder/NPs expelled from domain. The analysis TEM images are from Figures 3 and 4. NP-REF-30[30] and NP-REF-26[26] are representative results of neutral particles distribution in block copolymer.

NP/BCP hybrid materials in the presence of strong enthalpic interactions.

■ ASSOCIATED CONTENT

Supporting Information

The Supporting Information is available free of charge on the ACS Publications website at DOI: 10.1021/acs.macromol.5b02609.

PHOST and Au NPs synthesis, NP/BCP blend preparation, NPs ligand density calculation, NPs volume fraction in nanocomposite with particles loading, SAXS spectra of NP-16.0 and BCP blends (PDF)

■ AUTHOR INFORMATION

Corresponding Author

*E-mail: watkins@polysci.umass.edu (J.J.W.).

Notes

The authors declare no competing financial interest.

■ ACKNOWLEDGMENTS

This work is supported by the NSF Center for Hierarchical Manufacturing at the University of Massachusetts, Amherst (CMMI-1025020). The Materials Research and Engineering Center at University of Massachusetts Amherst supported facilities in this work. Authors acknowledge electron microscopy manager Alexander Ribbe, electron microscopy technician Louis Raboin, and nanotech and X-ray lab director Sekar Thirunavukkarasu for helpful discussions.

■ REFERENCES

(1) Balazs, A. C.; Emrick, T.; Russell, T. P. Nanoparticle Polymer Composites: Where Two Small Worlds Meet. *Science* **2006**, *314*, 1107−1110.

(2) Bockstaller, M. R.; Mickiewicz, R. A.; Thomas, E. L. Block Copolymer Nanocomposites: Perspectives for Tailored Functional Materials. *Adv. Mater.* **2005**, *17*, 1331−1349.

(3) Kao, J.; Thorkelsson, K.; Bai, P.; Rancatore, B. J.; Xu, T. Toward Functional Nanocomposites: Taking The Best of Nanoparticles, Polymers, and Small Molecules. *Chem. Soc. Rev.* **2013**, *42*, 2654−2678.

(4) Rosa, C. De; Auriemma, F.; Girolamo, R. Di; Pepe, G. P.; Napolitano, T.; Scaldaferri, R. Enabling Strategies in Organic Electronics Using Ordered Block Copolymer Nanostructures. *Adv. Mater.* **2010**, *22*, 5414−5419.

(5) Lopes, W. A.; Jaeger, H. M. Hierachical Self-Assembly of Metal Nanostructures on Diblock Copolymer Scaffolds. *Nature* **2001**, *414*, 735−738.

(6) Huynh, W. U.; Dittmer, J. J.; Alivisatos, A. P. Hybrid Nanorod-Polymer Solar Cells. *Science* **2002**, *295*, 2425−2427.

(7) Jaramillo, T. F.; Baeck, S. H.; Cuenya, B. R.; McFarland, E. W. Catalytic Activity of Supported Au Nanoparticles Depostied from Block Copolymer Micelles. *J. Am. Chem. Soc.* **2003**, *125*, 7148−7149.

(8) Xiang, J.; Lu, W.; Hu, Y.; Wu, Y.; Yan, H.; Lieber, C. M. Ge/Si Nanowire Heterostrctures as High Performance Field-Effect Transistors. *Nature* **2006**, *441*, 489−493.

(9) Huang, K.; Ma, H.; Liu, J.; Huo, S.; Kumar, A.; Wei, T.; Zhang, X.; Jin, S.; Gan, Y.; Wang, P. C.; He, S.; Zhang, X.; Liang, X. Size-Dependent Localization and Penetration of Ultrasmall Gold Nanoparticles in Cancer Cells, Multicellular Spheroids, and Tumors in Vivo. *ACS Nano* **2012**, *6*, 4483−4493.

(10) Ku, K. H.; Shin, J. M.; Kim, M. P.; Lee, C. H.; Seo, M. K.; Yi, G. R.; Jang, S. G.; Kim, B. J. Size-Controlled Nanoparticles-Guided Assembly of Block Copolymers for Convex Lens-Shaped Particles. *J. Am. Chem. Soc.* **2014**, *136*, 9982−9989.

(11) Link, S.; El-Sayed, M. A. Size and Temperature Dependence of the Plasmon Absoprtion of Colloidal Gold Nanoparticles. *J. Phys. Chem. B* **1999**, *103*, 4212−4217.

(12) Sarangi, S. N.; Hussain, A. M. P.; Sahu, S. N. Strong UV Absoprtion and Emission from L-cysteine Capped Monodispersed Gold Nanoparticles. *Appl. Phys. Lett.* **2009**, *95*, 073109.

(13) Choi, C. L.; Alivisatos, A. P. From Artificial Atoms to Nanocrystal Molecules: Preparation and Properties of More Complex Nanostructures. *Annu. Rev. Phys. Chem.* **2010**, *61*, 369−389.

(14) Talapin, D. V.; Lee, J. S.; Kovalenko, M. V.; Shevchenko, E. V. Prospects of Colloidal Nanocrystals for Electronic and Optoelectronic Applications. *Chem. Rev.* **2010**, *110*, 389−458.

(15) Brust, M.; Fink, J.; Bethell, D.; Schiffrin, D. J.; Kiely, C. Synthesis and Reactions of Functionalised Gold Nanoparticles. *J. Chem. Soc., Chem. Commun.* **1995**, 1655−1656.

(16) Brust, M.; Walker, M.; Bethell, D.; Schiffrin, D. J.; Whyman, R. Synthesis of Thiol-Derivatised Gold Nanoparticles in A Two-Phase Liquid-Liquid System. *J. Chem. Soc., Chem. Commun.* **1994**, 801−802.

(17) Jana, N. R.; Gearheart, L.; Murphy, C. J. Seeding Growth for Size Control of 5−40 nm Diameter Gold Nanoparticles. *Langmuir* **2001**, *17*, 6782−6786.

(18) Johnson, S. R.; Evans, S. D.; Brydson, R. Influence of A Terminal Functionality on the Physical Properties of Surfactant-Stablized Gold Nanoparticles. *Langmuir* **1998**, *14*, 6639−6647.

(19) Kanaras, A. G.; Kamounah, F. S.; Schaumburg, K.; Kiely, C. J.; Brust, M. Thioalkylated Tetraethylene Glycol: A New Ligand for Water Soluble Monolayer Protected Gold Clusters. *Chem. Commun.* **2002**, 2294−2295.

(20) Liu, X.; Xu, H.; Xia, H.; Wang, D. Rapid Seeded Growth of Monodisperse, Quasi-Spherical, Citrate-Stabilized Gold Nanoparticles via H_2O_2 Reduction. *Langmuir* **2012**, *28*, 13720−13726.

(21) Sabir, T. S.; Rowland, L. K.; Milligan, J. R.; Yan, D.; Aruni, A. W.; Chen, Q.; Boskovic, D. S.; Kurti, R. S.; Perry, C. C. Mechanistic Investigation of Seeded Growth in Triblock Copolymer Stabilized Gold Nanoparticles. *Langmuir* **2013**, *29*, 3903−3911.

(22) Shimizu, T.; Teranishi, T.; Hasegawa, S.; Miyake, M. Size Evolution of Alkanethiol-Protected Gold Nanoparticles by Heat Treatment in the Solid State. *J. Phys. Chem. B* **2003**, *107*, 2719−2724.

(23) Huh, J.; Ginzburg, V. V.; Balazs, A. C. Thermodynamic Behavior of Particle/Diblock Copolymer Mixtures: Simulation and Theory. *Macromolecules* **2000**, *33*, 8085−8096.

(24) Lee, J. Y.; Thompson, R. B.; Jasnow, D.; Balazs, A. C. Entropically Driven Formation of Hierachically Ordered Nanocomposites. *Phys. Rev. Lett.* **2002**, *89*, 155503.

(25) Thompson, R. B.; Ginzburg, V. V.; Matsen, M. W.; Balazs, A. C. Predicting the Mesophases of Copolymer-Nanoparticle Composites. *Science* **2001**, *292*, 2469−2472.

(26) Bockstaller, M. R.; Lapetnikov, Y.; Margel, S.; Thomas, E. L. Size-Selective Organization of Enthalpic Compatibilized Nanocrystals

DOI: 10.1021/acs.macromol.5b02609
Macromolecules 2016, 49, 3352−3360

in Ternary Block Copolymer/Particle Mixtures. *J. Am. Chem. Soc.* **2003**, *125*, 5276−5277.
(27) Kim, J. U.; O'Shaughnessy, B. Morphology Selection of Nanoparticle Dispersions by Polymer Media. *Phys. Rev. Lett.* **2002**, *89*, 238301.
(28) Yoo, M.; Kim, S.; Bang, J. Design and Fabrication of Thermally Stable Nanoparticles for Well-Defined Nanocomposites. *J. Polym. Sci., Part B: Polym. Phys.* **2013**, *51*, 494−507.
(29) Chiu, J. J.; Kim, B. J.; Kramer, E. J.; Pine, D. J. Control of Nanoparticle Location in Block Copolymer. *J. Am. Chem. Soc.* **2005**, *127*, 5036−5037.
(30) Chiu, J. J.; Kim, B. J.; Yi, G. R.; Bang, J.; Kramer, E. J.; Pine, D. J. Distribution of Nanoparticles in Lamellar Domains of Block Copolymers. *Macromolecules* **2007**, *40*, 3361−3365.
(31) Jang, S. G.; Kim, B. J.; Hawker, C. J.; Kramer, E. J. Bicontinuous Block Copolymer Morphologies Produced by Interfacially Acitve, Thermally Stable Nanoparticles. *Macromolecules* **2011**, *44*, 9366−9373.
(32) Kim, B. J.; Bang, J.; Hawker, C. J.; Chiu, J. J.; Pine, J.; Jang, S. G.; Yang, S.; Kramer, E. J. Creating Surfactant Nanoparticles for Block Copolymer Composites through Surface Chemistry. *Langmuir* **2007**, *23*, 12693−12703.
(33) Kim, S.; Yoo, M.; Kang, N.; Moon, B.; Kim, B. J.; Choi, S. H.; Kim, J. U.; Bang, J. Nanoporous Bicontinuous Structures via Addition of Thermally-Stable Amphiphilic Nanoparticles within Block Copolymer Templates. *ACS Appl. Mater. Interfaces* **2013**, *5*, 5659−5666.
(34) Jang, S. G.; Khan, A.; Hawker, C. J.; Kramer, E. J. Morphology Evolution of PS-*b*-P2VP Diblock Copolymers via Supramolecular Assembly of Hydroxylated Gold Nanoparticles. *Macromolecules* **2012**, *45*, 1553−1561.
(35) Jang, S. G.; Kramer, E. J.; Hawker, C. J. Controlled Supramolecular Assembly of Micelle-Like Gold Nanoparticles in PS-*b*-P2VP Diblock Copolymers via Hydrogen Bonding. *J. Am. Chem. Soc.* **2011**, *133*, 16986−16996.
(36) Lin, Y.; Daga, V. K.; Anderson, E. R.; Gido, S. P.; Watkins, J. J. Nanoparticle-Driven Assembly of Block Copolymers: A Simple Route to Ordered Hybrid Materials. *J. Am. Chem. Soc.* **2011**, *133*, 6513−6516.
(37) Yao, L.; Lin, Y.; Watkins, J. J. Ultrahigh loading of Nanoparticles into Ordered Block Copolymer Composites. *Macromolecules* **2014**, *47*, 1844−1849.
(38) Ye, T.; Chen, X.; Fan, X.; Shen, Z. Ordered Gold Nanoparticle Arrays Obtained with Supramolecular Block Copolymers. *Soft Matter* **2013**, *9*, 4715−4724.
(39) Yeh, S.; Wei, K.; Sun, Y.; Jeng, U.; Liang, K. S. Morphological Transformation of PS-b-PEO Diblock Copolymer by Selectively Dispersed Colloidal CdS Quantum Dots. *Macromolecules* **2003**, *36*, 7903−7907.
(40) Song, D. P.; Lin, Y.; Gai, Y.; Colella, N. S.; Li, C.; Liu, X. H.; Gido, S.; Watkins, J. J. Controlled Supramolecular Self-Assembly of Large Nanoparticles in Amphiphilic Brush Block Copolymers. *J. Am. Chem. Soc.* **2015**, *137*, 3771−3774.
(41) Enustun, B. V.; Turkevich, J. Coagulation of Colloidal Gold. *J. Am. Chem. Soc.* **1963**, *85*, 3317−3328.
(42) Tyagi, S.; Lee, J. Y.; Buxton, G. A.; Balazs, A. C. Using Nanocomposite Coatings To Heal Surface Defects. *Macromolecules* **2004**, *37*, 9160−9168.
(43) Kim, Y.; Chen, H.; Alexander-Katz, A. Free Energy Landscape and Localization of Nanoparticles at Block Copolymer Model Defects. *Soft Matter* **2014**, *10*, 3284−3291.

DOI: 10.1021/acs.macromol.5b02609
Macromolecules 2016, 49, 3352−3360